Article

Not peer-reviewed version

The Geological Investigation of the Lunar Reiner Gamma Magnetic Anomaly Region

Junhao Hu , Jingwen Liu , Jianzhong Liu * , Jiayin Deng , Sheng Zhang , Danhong Lei , Xuejin Zeng , Weidong Huang

Posted Date: 26 September 2024

doi: 10.20944/preprints202409.2046.v1

Keywords: Reiner Gamma; Lunar Magnetic Anomalies; 1:10,000 Regional Geological Map; Geomorphological Feature

Article

The Geological Investigation of the Lunar Reiner Gamma Magnetic Anomaly Region

Junhao Hu [1], Jingwen Liu [2], Jianzhong Liu [2,*], Jiayin Deng [3], Sheng Zhang [2], Danhong Lei [2], Xuejin Zeng [2] and Weidong Huang [2]

[1] School of Architectural Science and Engineering, Guiyang University, Guiyang, Guizhou, China
[2] Center for Lunar and Planetary Sciences, Institute of Geochemistry, Chinese Academy of Sciences, Guiyang, Guizhou, China
[3] Henan University of Science and Technology, School of Civil Engineering and Architecture, Henan, China
* Correspondence: liujianzhong@mail.gyig.ac.cn; Tel.: +86-18786617851

Abstract: Reiner Gamma is a potential target for low-orbiting spacecraft or even surface-landed missions in the near future. Unfortunately, thus far no comprehensive low altitude (below 20 km) or surface measurements of the magnetic field, magnetic source and plasma environment have been made post-Apollo to complement and complete our understanding of the solar wind interaction with lunar magnetic anomalies and swirl formation. Acquiring the detailed geological knowledge of the Reiner Gamma region is significant for the above scientific targets. In this study, the following research work in the lunar Reiner Gamma magnetic anomaly region was carried out for the regional geological investigation: (1) the topographic and geomorphologic analysis; (2) elements, minerals and sequence analysis; (3) 1:10,000 regional geological map analysis. Our work helps define measurement requirements for possible future low-orbiting or surface-landed missions to the Reiner Gamma area or similarly magnetized regions of the lunar surface.

Keywords: reiner gamma; lunar magnetic anomalies; 1:10,000 regional geological map; geomorphological feature

1. Introduction

Although the Moon today does not have a global magnetic field, the research on remanent magnetization in lunar rocks and crust demonstrated that there was a substantial lunar surface field billions of years ago [1–7]. The key scientific issues including the lunar heat loss [1,8], basic dynamo theory of the lunar core and mantle [4,6], the presence of volatiles on the surface on the poles [9–11], and possibly paleo-solar wind studies [9,12] may be hopeful of resolving based on the understanding of the origin, intensity, and life-time of this global field. The magnetic anomalies fields have been detected over numerous portions of its crust, and most of these regions are located antipodal to large basins [2,13–21]. The dominant genesis hypothesis of these magnetic anomaly fields includes ejecta deposits [21–26], thermoremanent magnetization from magmatic processes [2,9,27–30], and through shock-remanent magnetization by large impacts [24,31]. Obtaining information about the magnetic source bodies of these anomalies involve the geometry, depth, formation time and magnetic mineralogy can better constrain the timing and the strength of the lunar past dynamo field [5,9,21,29,32,33].

The lunar swirls, characterized by the sinuous pattern of albedo in the soil, play a valuable tool in investigating the Moon's lithospheric magnetic anomalies, due to its unique geologic features with magnetic and photometric anomalies [5,9,29,34–36]. Several mechanisms have been proposed for swirl formation including cometary impact effects [37], solar wind deflection model [38,39], electrostatic dust levitation and transport [40–42] and the magnetic sorting [43]. The above hypotheses usually involved a "mini-magnetosphere" that shields the surface from the darkening effects of the solar wind [35,38,44–47]. Moreover, the lunar swirls can be used to more carefully

 doi:10.20944/preprints202409.2046.v

investigate the geometry, depth, and formation time of the source bodies, attributed to the shallow burial scale of the magnetic anomaly source body [5,28,29].

Reiner Gamma, located on the lunar nearside along the western edge of Oceanus Procellarum (center: 7.4° N, 301° E) (**Figure 1**), is perhaps the most well-known magnetic anomaly with 22 nT at 30 km altitude [20,48–51], but no theory for its formation has been accepted [14,26,28,29,32,52,53]. Moreover, the spatial resolutions of the GRAIL gravity map and modeling are insufficient to resolve the narrow (<1–5 km width) dike features that might be responsible for swirls [2] and the low-altitude with high-resolution lunar magnetic field measurements and surface field sampling at Reiner Gamma region are still in the blank [9,36,48,54], which lead to the genesis debated of this magnetic anomaly. Therefore, the comprehensive geological investigation of this typical lunar swirls region is necessary for future surface-landed missions and low-altitude measurements, which would also provide an opportunity to determine with much higher accuracy the strength and direction of the dynamo field when Reiner Gamma formed [2,9]. To acquire the detailed geological background of the Reiner Gamma region, the following research in this region were carried out: (1) topographic and geomorphologic analysis; (2) elements, minerals and sequence analysis; (3) 1:10,000 regional geological maps analysis. Our work could provide basic cognition for the surface-landed missions and further to constrain the geometry, depth, and formation time of the source bodies, which may solve the geologic processes that led to the formation of crustal magnetism and the type of dynamo that magnetized them.

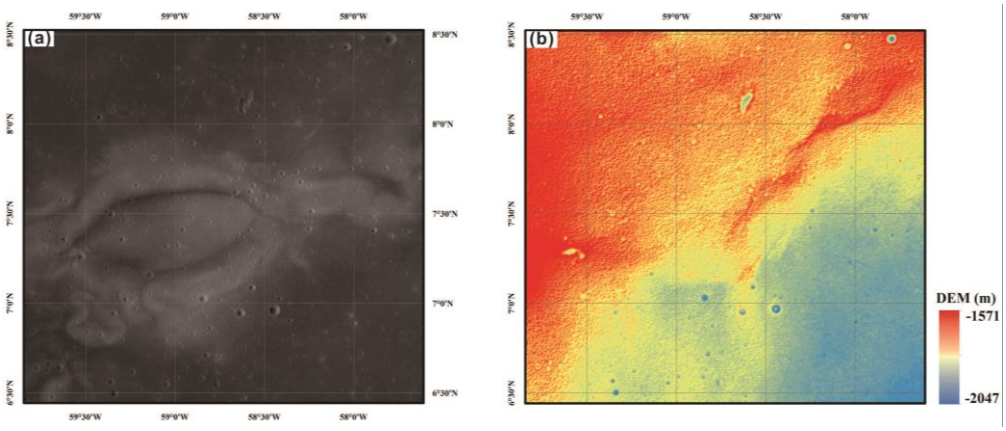

Figure 1. The NAC and DEM maps in Reiner Gamma region.

2. Data and Methods

2.1. Geochemical Composition Data

The Kaguya Multiband Imager acquired data in 9 ultraviolet–visible (UVVIS) to near-infrared (NIR) spectral bands (415, 750, 900, 950, 1001, 1000, 1050, 1250, 1550 nm), and covers the range from 65°N ~ 65°S on the lunar surface. The instrument provided a spatial resolution of ~20 m per pixel for the first five spectral bands (UVVIS, 415–1001 nm), and ~62 m per pixel for the last four (NIR, 1000–1550 nm) at the nominal altitude of 100 km [55]. In this study, the abundances of the minerals (e.g., olivine, low/high-calcium pyroxene and plagioclase) and the submicroscopic iron (SMFe) in Reiner Gamma magnetic anomaly region were from Lemelin et al. [55,56] and Taylor et al. [57], which were based on the MI data, respectively. Moreover, Lemelin et al. [55] downsampled the UVVIS data to the same spatial resolution as the NIR (~62 m per pixel) so that they could work with 9 spectral bands with matching spatial resolution. They also corrected systematic differences in the reflectance spectra between the first five spectral bands (UVVIS data) and the last four (NIR data) due to the differences in data source, and this data reduction method is explained in detail in Lemelin et al. [56].

Meanwhile, the abundances of the five major oxides (e.g., MgO, FeO, Al_2O_3, CaO and TiO_2) in this study were from Zhang et al. [58]. To obtain good the correlation between MI spectral reflectance values and oxide content, the 1D-CNN algorithm was used in Zhang et al. [58]. Different from the MI data used in Lemelin et al. [55] and Taylor et al. [57], Zhang et al. [58] used the eight bands (415 nm,

 doi:10.20944/preprints202409.2046.v

750 nm, 900 nm, 950 nm, 1001 nm, 1050 nm, 1250 nm, and 1550 nm) of the MI global mosaic for the calculation of the abundances of the five major oxides.

2.2. Topographic and Geomorphological Analysis Method

At present, the direct method for obtaining planetary topography is using a laser altimeter to send laser pulses from orbit and time the returning pulses [59–61]. In this study, the elevation data were obtained from the Chang'E-2 DEM, Lunar Orbiter Laser Altimeter (LOLA) [61,62] and the high-resolution SLDEM2015 [63]. The LOLA supplied highly accurate global coverage with a vertical precision of ~10 cm and an accuracy of ~1 m [61,62]. Furthermore, the resolution of LOLA is approximately 118 meters per pixel. The SLDEM was combined by the LOLA and the SELENE TC data through the Kaguya teams and covers latitudes within ±60° with a horizontal resolution of ~59 meters per pixel and a vertical accuracy of ~3 to 4 m [63]. In addition, the high-resolution image data were from Chang'E-2 and narrow-angle camera images (LROC NAC, with the resolution of approximately 0.5 meters/pixel). Considering the data resolution and the data size of subsequent data processing, this study used the DEM generated by LOLA to study the classification criteria of lunar relief amplitude in the target area of the Reiner Gamma region. The higher-resolution SLDEM data were used to verify the optimum ranges of the lunar relief amplitude calculated from the LOLA DEM. And the data were downloaded from https://planetarymaps.usgs.gov/mosaic/Lunar_LRO_LOLA_Global_LDEM_118m_Mar2014.tif and https://astrogeology.usgs.gov/search/map/Moon/LRO/LOLA/Lunar_LRO_LOLAKaguya_DEMmerge_60N60S_512ppd.

The slope and the roughness in the target area of the Reiner Gamma region were calculated from the elevation data. Thresholds of -2500 m, -1500 m, 1000 m, and 3000 m were used as elevation criteria in this study's lunar morphological classification system. The lunar surface is divided into five geomorphic types including very low altitude, low altitude, medium altitude, high altitude and very high altitude [64]. Based on the LOLA data, this study calculates slope data for the Reiner Gamma region through the maximum average method [65]. Referring to general classification standards for Earth's topographic slopes, areas on the lunar surface are categorized as follows: less than 0.5° as considered plains, 0.5-2° as gentle slopes, 2-5° as gradual slopes, 5-15° as moderate slopes, 15-35° as steep slopes, 25-55° as rugged slopes and 55-90° as vertical slopes. This study quantitatively analyzes the roughness of the Reiner Gamma region using the root mean square height difference method through the elevation data from Chang'E-2, which has a resolution of 20 meters and the method employed a 20-meter baseline [66].

For calculating the relief amplitude in this region, we determine the best window for relief amplitude calculation through the mean change-point method based on the Chang'E-2 20-meter DEM data [67]. In general. the corresponding landforms in lunar surface are classified into seven types (e.g., minor microrelief plains, minor microrelief platforms, microrelief landforms, small relief landforms, medium relief landforms, large relief landforms and extremely large relief landforms) according to relief amplitudes of 100 m, 200 m, 300 m, 700 m, 1500 m, and 2500 m [67]. The rock abundance in this study is inferred from Diviner data obtained by LRO during its circular orbit phase from October 3, 2009 to October 7, 2011. Each pixel represents the fractional area fragments occupy within that lunar surface area. The algorithm considers the influence of local slopes on rock abundance inversion based on DEM terrain data acquired by LOLA [68]. Ultimately, this study delineates suitable areas for lunar surface-landed activities based on a comprehensive acquisition of terrain and landform characteristics within the Reiner Gamma region.

2.3. Mapping the 1:10,000 Geological Map

Chinese researchers have completed the compilation of the 1:2.5 Million Lunar Geological Map and achieved remarkable international recognition including the lunar geological maps, the lunar lithologic maps and the lunar tectonic maps [69–73]. Based on the 1:2.5 Million Lunar Geological Map, we have mapped out the geologic structures, rocks and crater units in the target of the Reiner Gamma

 doi:10.20944/preprints202409.2046.v

region with 1:10,000-scale through the high-resolution geochemical composition data, image data and the DEM data collected and produced in 2.1 and 2.2.

The main mapping processes are as follows: (1) Scale determination: the decision to use a 1:10,000 scale for the Reiner Gamma region was carefully considered to balance the need for detailed geological information with the practical limitations of data resolution and map readability. (2) Determination of map content representation: this included not only all the geological structures in the 1:2.5 Million Lunar Geological Map but also the magnetic anomaly bands in this region. (3) Development of standards and specifications for legends and symbols: the majority of the legends and symbols were inherited from the 1:2.5 Million Lunar Geological Map with the modifications made to represent lunar ridges and rilles as areal structures. Additionally, graphical legends for magnetic anomaly bands have been included. (4) Establishment of base map databases: through the ArcGIS, we have created a gdb (geodatabase) file and subsequently established multiple feature classes based on the attribute tables and classifications of geological units from the 1:2.5 Million Lunar Geological Map. Each feature class will correspond to a specific geological unit, thereby organizing the data into distinct groups of feature types. (5) Geological mapping: identification and expression of lunar structures, igneous rocks, impact ejecta and the age of various factors. (6) Map compilation: establish a mapping template based on the ArcGIS; graphic editing of the map units; label to annotation. (7) Quality control: topology checking and manual checking. (8) Map finalization and output.

2.4. Stratigraphic Analysis of the Reiner Gamma Region

To conduct stratigraphic analysis within the Reiner Gamma region, we first obtained the distribution maps of the major minerals including plagioclase, pyroxene, and olivine through the multispectral remote sensing data. Next, we combined the above information and the elevation data to divide geological units of the basalts in the study area. Finally, we performed absolute geological dating based on the size-frequency distribution of impact craters overlaying these units. The detailed steps are presented as follows: (1) Extract the identification markers including raised positive landforms, impact melt and vertical profiles of crater walls from the rims or continuous ejecta blankets of the corresponding large impact craters; (2) Identify geological units for future surface-landed mission within Reiner Gamma by analyzing the topographic relief, morphology, roughness and the distribution of material composition in studied area; (3) Extract the main impact craters above and establish buffer zones based on the preservation status of crater rims; (4) Perform period analysis based on lunar geological period curves and establish the stratigraphic relationships within the Reiner Gamma region (http://priede.bf.lu.lv/GIS/.Descriptions/RST/Sect19/nicktutor_19-5.shtml).

3. Results

3.1. Geochemical Compositions in the Reiner Gamma Region

As shown in the **Figure. 2a-e**, the MgO content ranges from 5.1 to 13.5 wt%, FeO content ranges from 6 to 23 wt%, Al_2O_3 content ranges from 9.5 to 21.2 wt%, CaO content ranges from 9.3 to 13.2 wt% and TiO_2 content ranges from 2.5 to 9.6 wt%. Compared to the dark lanes of the Reiner Gamma swirl and the surrounding mare regions, the bright lobes of the swirl have higher contents of MgO, CaO, Al_2O_3, and significantly lower FeO, TiO_2 and submicroscopic iron (SMFe) contents (**Figure 2**). The contents of olivine, orthopyroxene, clinopyroxene, plagioclase, and SMFe are 0-48 wt%, 0-74 wt%, 0-60.8 wt%, 14-63 wt%, and 0.5-7 wt%, respectively (**Figures 2f, 3a-d**). The bright labels of the swirl have lower contents of olivine, orthopyroxene and clinopyroxene and higher contents of plagioclase compared to the dark lanes of the Reiner Gamma swirl and the surrounding mare regions (**Figure 3a-d**).

 doi:10.20944/preprints202409.2046.v

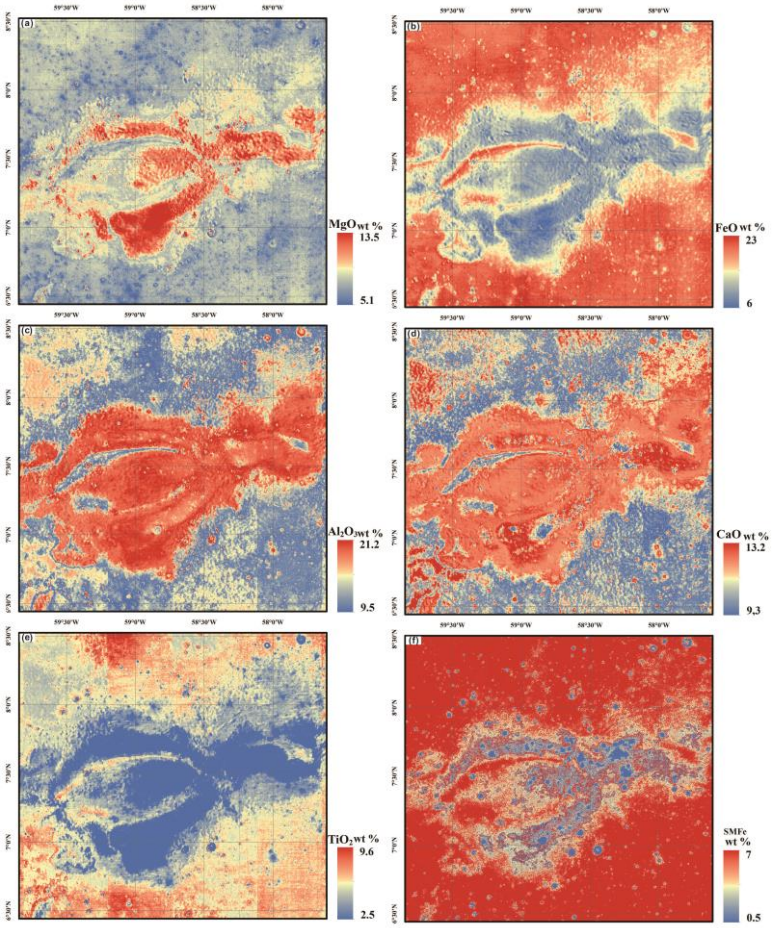

Figure 2. The major element compositions in the Reiner Gamma region.(a)-(f) represent the MgO, FeO, Al_2O_3, CaO, TiO_2 and SMFe contents in Reiner Gamma region, respectively.

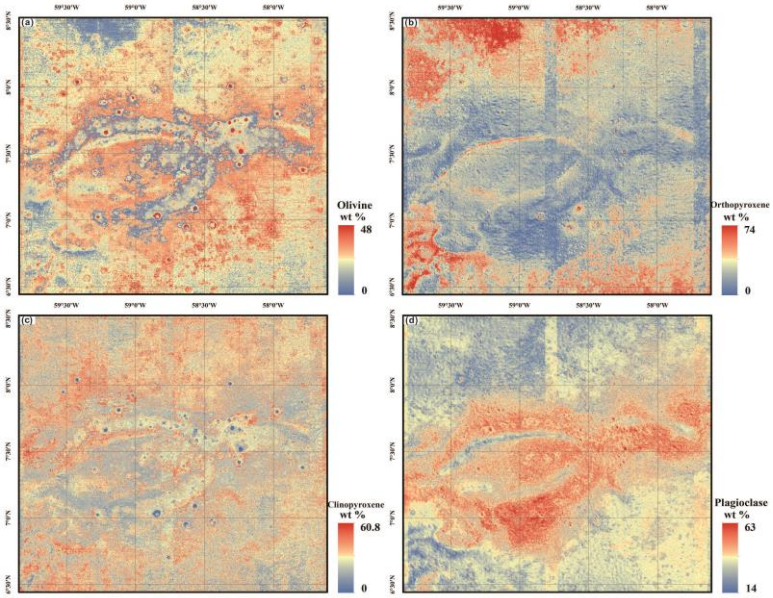

Figure 3. The major mineral compositions in the Reiner Gamma region. (a)-(d) represent the Olivine, Orthopyroxene, Clinopyroxene and Plagioclase contents in Reiner Gamma region, respectively.

 doi:10.20944/preprints202409.2046.v

3.2. Topographic and Geomorphological Parameters of the Target in Reiner Gamma Region

The Reiner Gamma magnetic anomaly area belongs to a low-altitude region with the elevation ranging from -2041 m to -1548 m (**Figure 1b**). The eastern region of this Lunar swirl is suitable for surface-landed missions due to its high quality in geological characters (**Figure 4a**). It ranges from -1833.96 m to -1685.96 m in altitude (**Figure 4b**). From view of the slope map (**Figure 4c**), it is evident that the slopes in this region vary moderately with most parts ranging from 0 to 5 degrees over a large extent, and smaller parts ranging from 5 to 15 degrees. The roughness values overall range between 0 and 1.5 m with some local areas exceeding 1.5 m (**Figure 4d**). Additionally, there are 58 craters larger than 300 meters in diameter which indicates a relatively low crater density in this region (**Figure 4a**). The average rock abundance is 5.5, with a maximum value of 67% which suggest a low rock abundance (**Figure 4e**). From the basic landform types (**Figure 4f**), the blue areas represent minor microrelief plains with the highest safety level which cover the majority of the map, the yellow areas represent microrelief landforms with some degree of hazard which just sparsely distributed on the map, and the red areas represent small relief landforms which are the most dangerous regions, but are extremely limited in distribution.

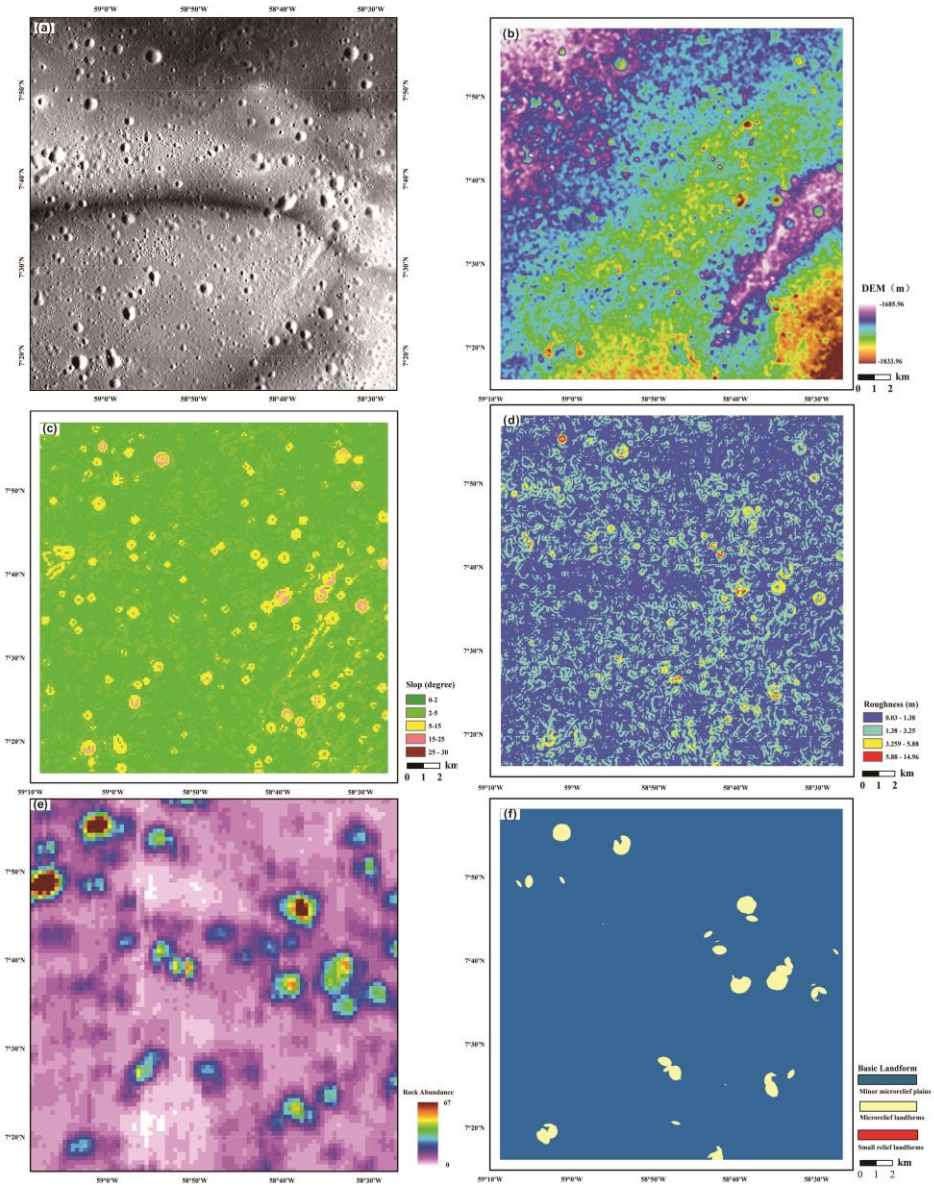

Figure 4. Topographic and geomorphological parameters in the target of the Reiner Gamma Region. (a)-(b) represent NAC and DEM maps in the target of the Reiner Gamma Region. (c)-(f) represent the

 doi:10.20944/preprints202409.2046.v

slop, roughness, rock abundance and basic landforms in the target of the Reiner Gamma Region, respectively.

3.3.1:10,000. Geological Map of the Target in Reiner Gamma Region

Combining imaging data with a resolution better than 3 meters, DEM with a spatial resolution better than 20 meters and the compositional data, the 1:10,000 geological map of the target area in the Reiner Gamma magnetic anomaly region (20 km by 20 km) has been created (**Figure 5**). This geological map includes 60,319 impact craters with diameters ranging from 10 to 100 meters. There are 934 crater materials of Copernican Period with diameters over 100 meters, 585 crater materials of Eratosthenian Period with diameters over 100 meters, 12 crater materials of undivided age with diameters over 100 meters, and 55 crater materials of Imbrian Period with diameters over 100 meters. This map also composes 1 basalt unit, 4 linear ridge structures, 6 domes and 24 impact crater chains (**Figure 5**).

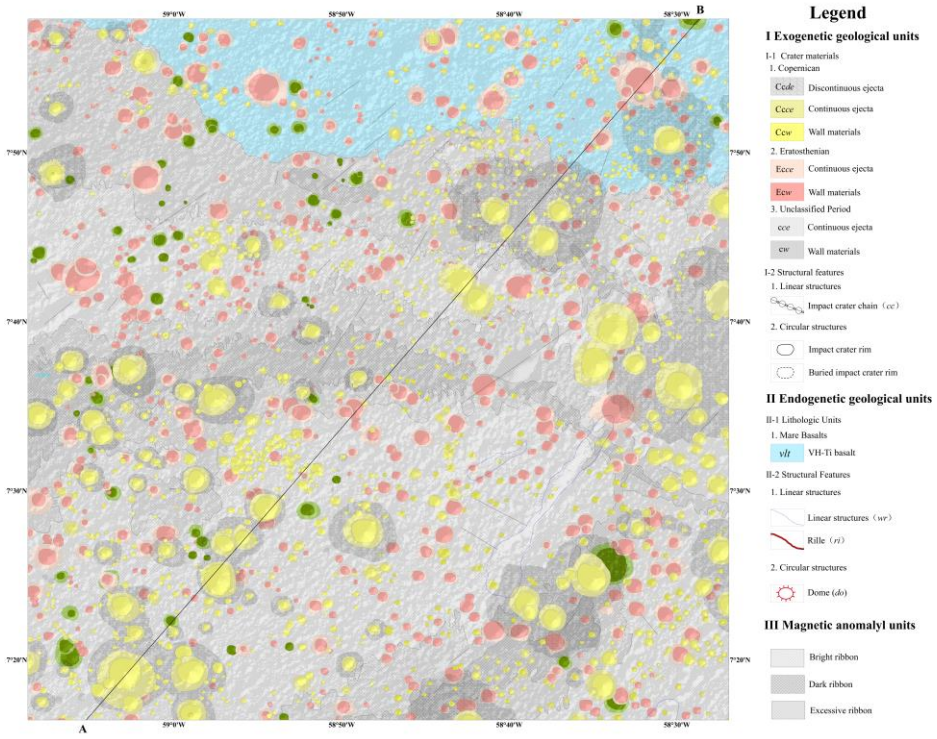

Figure 5. The 1:100,00 geologic map of the target in the Reiner Gamma Region.

3.4. The Stratigraphic Sequence within the Target of the Reiner Gamma Region

As shown in **Figure 6**, the lowest layer in this area is composed of ferroan anorthosites formed in the Magma-oceanian Period. During the Aitkenian Period, the Reiner Gamma region experienced continuous ejecta deposition from the Grimaldi basin to the southwest and the Flamsteed-Billy basin to its southeast, which overlayed the ferroan anorthosites. No material from the Nectarian or Imbrian Period was observed in the Reiner Gamma region. Following the formation of the Imbrium basin, extensive volcanic activities occurred in this region during ~3.9 Ga to 3.5 Ga [74,75]. Subsequently, a small-scale eruption of low-titanium basalts occurred in the Reiner Gamma region (3.30 Ga) [75]. During the later modification stage (3.16 Ga to the present), the basalts underwent modification from small-scale impact events and space weathering, which generated various types of impact craters in the region. Due to the differences in surface lithology and the alteration resulting from space weathering, significant differences in the thickness of surface regolith are observed in the basaltic and volcanic breccia areas [76].

 doi:10.20944/preprints202409.2046.v

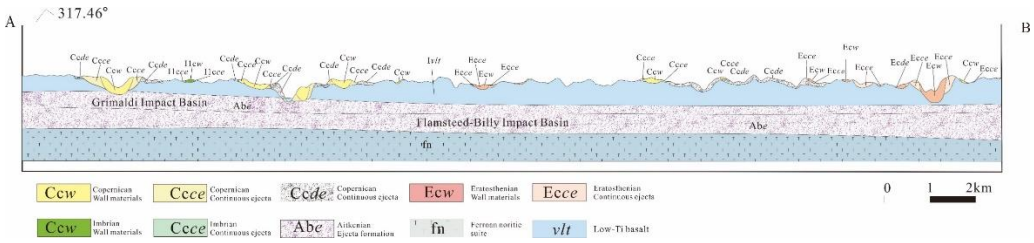

Figure 6. The stratigraphic sequence of the target in the Reiner Gamma Region.

4. Discussion

4.1. Geochemical Features of the Reiner Gamma Region

Recent studies have proposed that the formation of the Reiner Gamma swirl may be related to the interaction between the mini-magnetosphere and the solar wind plasma [12,34,43,47,77,78], and the optical anomalies in this region are primarily attributed to differences in lunar soil maturity [34,79]. **Figures. 2** and **3** show no significant differences in the element contents and mineral compositions between the dark lanes of the Reiner Gamma swirl and the surrounding lunar mare, which is in accordance with similar spectral characteristics [79]. However, the bright lobes of Reiner Gamma have higher MgO, Al_2O_3, and CaO contents and lower FeO, TiO_2 contents compared to the dark lanes and the surrounding lunar mare (**Figure 2a-e**). Additionally, the bright lobes have lower olivine, orthopyroxene and clinopyroxene contents, but higher plagioclase content compared to the above regions (**Figure 3**). These characteristics are also reflected in the spectral and photometric differences among the bright lobes, dark lanes and the surrounding lunar mare [35,79]. Besides, the bright lobes of the Reiner Gamma swirl have significantly lower SMFe content compared to the dark lanes and the surrounding lunar mare (**Figure 2f**). The features above may corroborate that the reflectance differences of the swirls are related to the interaction between the mini-magnetosphere and the solar wind plasma [47,78,80,81].

Existing research have shown the presence of ellipsoidal magnetic sources within the basalt in this area [2,5], and the types of magnetic minerals within these sources can reflect their origins [2,82–86]. However, the thickness of the overlying basalts with ~ 250 m to ~ 2.3 km [5] and the spatial resolution of the existing gravity data make it challenging to distinguish the origin of these magnetic sources [2], whether they are the melt sheet or floor deposits of an impact crater, or slow cooling and sub-solidus reduction of lunar magmatic bodies. Therefore, surface-landing for the measurements of the field and plasma at Reiner Gamma is significant for knowing the magnetic mineralogy of the source bodies and further provides an opportunity to determine with much higher accuracy the strength and direction of the dynamo field when Reiner Gamma formed [2,9,40].

4.2. Topographic and Geomorphological Features of the Target in the Reiner Gamma Region

The topographic and geomorphological features of the lunar surface are crucial for future surface-landed missions. The elevation and relief amplitude as the macroscopic morphological types reflect lunar terrain variations through composite matrices. The elevation variations of the target in the Reiner Gamma region range from -1833.96 m to -1685.96 m, which indicate this area belongs to the low-altitude area (**Figure 4b**). Simultaneously, in the view of the basic landform types (**Figure 4f**), it is evident that the minor microrelief plains dominate most of the target region. Moreover, the slightly hazardous microrelief landforms areas occurrences sporadic, and the most hazardous regions of small relief landforms are only found in extremely isolated areas.

The slope and roughness are essential indicators for expressing terrain characteristics. The magnitude of the slope directly impacts the scale and intensity of surface material flow and energy conversion, which represents the local surface inclination. The target in the Reiner Gamma region is classified as gentle to gradual slopes, which exhibits slopes ranging broadly from 0 to 5°, with smaller areas having slopes between 5 and 15° (**Figure 4c**). Surface roughness serves as a crucial parameter in assessing the engineering feasibility of ground operations. It quantifies the degree of lunar surface

 doi:10.20944/preprints202409.2046.v

erosion and spatial variations in lunar morphology and records geological activities such as erosion, subsidence, deposition and infilling on planetary surfaces. As shown in **Figure. 4d**, the roughness values in the target of the Reiner Gamma region range predominantly from 0 to 1.5 meters with some local areas exceeding 1.5 meters, which indicates the selected target is located in flat terrain. From the view of **Figure. 4e**, the rock abundance is relatively low except for a few areas with 5.5% on average and 67% on maximum value.

Moreover, there are only 58 impact craters larger than 300 meters in diameter, which indicates a low crater density in this region. Meanwhile, four major wrinkle ridges oriented in a northeast direction are located on the bright streaks on the eastern side of the Reiner Gamma swirl. Other features including grooves, rilles and grabens are relatively small in scale (**Figure 5**). In summary, the geological environments in the selected target are generally stable and mainly influenced by the infilling of mare basalts with relatively small-scale structural types and few surrounding impact basin. Therefore, this target is highly favorable for surface-landing and in-situ measurements of both magnetic fields and plasma within lunar crustal magnetic anomalies, which help to understand the nature of anomalies and the various processes involved in space weathering.

4.3. Geological Evolution of the Reiner Gamma Region

4.3.1. Magma-Oceanian and Aitkenian Periods

Crystallization of the lunar magma ocean (LMO) led to differentiation of the silicate portion into a dense ultramafic to mafic cumulate pile (the lunar mantle), and after ~ 70 - 80 percent solidification, the crystallization of plagioclase to form anorthosite flotation crust that ultimately reached a thickness of up to ~60 km [40,87–92], the crust in this region is presented in **Figure 6**. At a late stage (> 90 PCS), a residual melt enriched in highly incompatible elements, including the heat-producing elements K, Th and U, represents the source of the geochemical signature identified in various lunar lithologies (e.g. KREEP basalts) [91,93–96]. New laboratory and spacecraft measurements strongly indicate that the intensity of the magnetization originated from an ancient core dynamo reached that of the present Earth during 4.25 to 3.56 billion years ago (Ga) [6,7,32]. The mechanisms for sustaining such an intense and long-lived dynamo are uncertain but may include mechanical stirring by the mantle and core crystallization [6]. During the Aitkenian Period (4.31 - 3.92 Ga), continuous ejecta from the Grimaldi basin to the southwest and the Flamsteed-Billy basin to the southeast of the Reiner Gamma region, were deposited onto the studied area, covering the primordial lunar crust composed of ferroan anorthosites.

4.3.2. Nectarian and Imbrian Periods (3.88~3.16 Ga)

No Nectarian Period rocks were exposed in the Reiner Gamma region. Furthermore, large-scale volcanic eruptions occurred in the area after the formation of the Mare Imbrium basin (~3.9 Ga - 3.5 Ga) [74,75,97,98]. Meanwhile, this period of volcanic activity coincides with the era of high magnetic fields on the Moon [6,9,32]. Subsequently, a small-scale low-titanium basaltic magma eruption occurred in the study region (~3.30 Ga) [75], and the field then declined by at least an order of magnitude by ~ 3.3 Ga [6,99–101]. Recent studies have suggested that the source of the magnetic anomaly in the Reiner Gamma region was located in the lower part of this low-titanium basalt, with the formation time between ~ 3.3 Ga and ~ 3.9 Ga, and the burial depth ranging from ~ 250 m to ~ 2.3 km [5,28,29]. The basal magnetic source might originate from thermoremanent magnetization generated by subsolidus-reduction associated with magmatic activity [2,5,28,51], or it could be related to a uniformly magnetized elliptical disk form from the melt sheet or floor deposits of an impact crater [9,21,26,52]. At the current stage, the spatial resolutions of the GRAIL gravity map and modeling are insufficient to resolve the narrow (< 1 - 5 km width) dike features that might be responsible for swirls [2]. Therefore, surface landing could provide opportunities to constrain the magnetic source bodies' geometries and even the lunar dynamo's evolution.

 doi:10.20944/preprints202409.2046.v

4.3.3. Eratosthenian and Copernican Periods

After the mare basalt infilling process, the surface of the Reiner Gamma region was modified by small impact events and space weathering, which formed the various types of impact craters. Due to the differences in surface rock composition, distinct thicknesses of lunar regoliths have formed in the basalt and volcanic breccia regions [76]. The Marius Hills located northwest (~150 km) of the Reiner Gamma swirl experienced continuous volcanic activity during 1.03 - 3.65 Ga [102,103], with the volcanic activity in the region near the tail of the Reiner Gamma swirl occurring between 1.3 - 3.3 Ga [102]. Reiner Gamma's magnetic source bodies were also demagnetized by the heat from volcanic domes in the Marius Hills during this time [5,102], which may indicate that the dynamo that was only episodically strong [1], or the dynamo that existed in a weakened state [104].

5. Conclusions

The selected target for future surface-landing is located in the eastern of the Reiner Gamma magnetic anomaly region. This target belongs to the low-altitude area, and most of which are located in minor microrelief plains. The geological environments in this area are generally stable and mainly influenced by the infilling of mare basalts with relatively small-scale structural types and few surrounding impact basin. Meanwhile, this target include both the bright lobes and dark lanes of the Reiner Gamma. Therefore, in the view of the geological and geochemical features, the target can be a possible future low-orbiting or surface-landed mission for understanding the nature of magnetic anomalies and the various processes involved in space weathering.

Author Contributions: Conceptualization, J.H. (Junhao Hu), J.L. (Jingwen Liu) and J.L. (Jianzhong Liu).; methodology, J.D. (Jiayin Deng).; software, J.L. (Jingwen Liu).; validation, J.H. (Junhao Hu) and J.L. (Jingwen Liu).; formal analysis, J.L. (Jingwen Liu); investigation, J.L. (Jingwen Liu), D.L (Danhong Lei), S.Z (Sheng, Zhang), W.H (Weidong, Huang) and X.Z (Xuejin Zeng); resources, J.L. (Jingwen Liu); data curation, J.L. (Jingwen Liu).; writing—original draft preparation, J.H. (Junhao Hu) and J.L. (Jingwen Liu); writing—review and editing, J.H. (Junhao Hu), J.L. (Jingwen Liu) and J.L. (Jianzhong Liu); visualization, J.L. (Jingwen Liu); supervision, J.L. (Jianzhong Liu); project administration, J.L. (Jianzhong Liu); funding acquisition, J.L. (Jianzhong Liu). All authors have read and agreed to the published version of the manuscript.

Funding: This work was funded by the Supported by the National Key Research and Development Program of China (Grant No. 2022YFF0503100), Compilation of Chinese Regional Geological Chronicles and Series of Maps, Grant NO DD20221645, Guizhou Provincial Basic Research Program (Qian Ke He basic-ZK [2021] general type 206 and Qian Ke He basic-ZK [2024] general type 670), Guizhou Provincial Department of Education Higher Education Young Science and Technology Talent Growth Program (Qian Jiao He KY[2020]077), and Guiyang University PhD start-up grant (2019039510821).

Data Availability Statement: The LOLA DEM, LROC WAC, LROC NAC, SLDEM2015 and the abundance of olivine, low-calcium pyroxene, high-calcium pyroxene, plagioclase,submicroscopic iron (SMFe) can be accessed through the Planetary Data System Geosciences Node (https://pds-geosciences.wustl.edu/dataserv/moon.html).

Acknowledgments: The authors are grateful to Dr. Jing-Wen Liu and Prof. Jian-Zhong Liu for their great contribution to the conception and experimental support of this study. Many thank to the Dr. Jia-Yin Deng for her data methods and Engineer Sheng Zhang, Dan-Hong Lei, Xue-Jin Zeng and Wei-Dong Huang for their data analysis.

Conflicts of Interest: The authors declare no conflicts of interest.

References

1. Evans, A.J.; Tikoo, S.M. An episodic high-intensity lunar core dynamo. Nature Astronomy 2022, 6, 325-+, doi:10.1038/s41550-021-01574-y.
2. Liang, Y.; Tikoo, S.M.; Krawczynski, M.J. Possibility of Lunar Crustal Magmatism Producing Strong Crustal Magnetism. J Geophys Res-Planet 2024, 129, doi:10.1029/2023JE008179.
3. Mighani, S.; Wang, H.P.; Shuster, D.L.; Borlina, C.S.; Nichols, C.I.O.; Weiss, B.P. The end of the lunar dynamo. Science Ad-vances 2020, 6, eaax0883, doi:10.1126/sciadv.aax0883.
4. Scheinberg, A.L.; Soderlund, K.M.; Elkins-Tanton, L.T. A basal magma ocean dynamo to explain the early lunar magnetic field. Earth and Planetary Science Letters 2018, 492, 144-151, doi:10.1016/j.epsl.2018.04.015.

5. Seritan, M.R.K.; Garrick-Bethell, I. Volcanic thermal demagnetization of the Reiner Gamma magnetic anomaly. Icarus 2023, 403, 115601, doi:10.1016/j.icarus.2023.115601.
6. Weiss, B.P.; Tikoo, S.M. The lunar dynamo. Science 2014, 346.
7. Zhai, K.; Yin, Y.; Zhai, S.M. Thermal and Dynamo Evolution of the Lunar Core Based on the Transport Properties of Fe-S-P Alloys. Geophysical Research Letters 2024, 51, doi:10.1029/2024GL108131.
8. Evans, A.J.; Tikoo, S.M.; Andrews-Hanna, J.C. The Case Against an Early Lunar Dynamo Powered by Core Convection. Geophysical Research Letters 2018, 45, 98-107, doi:10.1002/2017gl075441.
9. Garrick-Bethell, I.; Poppe, A.R.; Fatemi, S. The Lunar Paleo-Magnetosphere: Implications for the Accumulation of Polar Volatile Deposits. Geophysical Research Letters 2019, 46, 5778-5787, doi:10.1029/2019gl082548.
10. Green, J.; Draper, D.; Boardsen, S.; Done, C.F. When the Moon had a magnetosphere. Science Advances 2020, 6, doi:10.1126/sciadv.abc0865.
11. Tarduno, J.A.; Cottrell, R.D.; Lawrence, K.; Bono, R.K.; Huang, W.T.; Johnson, C.L.; Blackman, E.G.; Smirnov, A.V.; Nakaji-ma, M.; Neal, C.R., et al. Absence of a long-lived lunar paleomagnetosphere. Science Advances 2021, 7, doi:10.1126/sciadv.abi7647.
12. Poppe, A.R.; Garrick-Bethell, I.; Fatemi, S. Fractionation of Solar Wind Minor Ion Precipitation by the Lunar Paleomagne-tosphere. The Planetary Science Journal 2021, 2, doi:10.3847/PSJ/abea7d.
13. Baek, S.M.; Kim, K.H.; Garrick-Bethell, I.; Jin, H. Magnetic Anomalies Within the Crisium Basin: Magnetization Directions, Source Depths, and Ages. J Geophys Res-Planet 2019, 124, 223-242, doi:10.1029/2018je005678.
14. Hood, L.L.; Torres, C.B.; Oliveira, J.S.; Wieczorek, M.A.; Stewart, S.T. A New Large-Scale Map of the Lunar Crustal Magnet-ic Field and Its Interpretation. J Geophys Res-Planet 2021, 126, doi:10.1029/2020JE006667.
15. Lee, J.K.; Maxwell, R.; Jin, H.; Baek, S.M.; Ghassemi, O.; Kelley, M.; Lee, H.; Kim, K.H.; Lee, S.; Garrick-Bethell, I. A small lunar swirl and its implications for the formation of the Reiner Gamma magnetic anomaly. Icarus 2019, 319, 869-884, doi:10.1016/j.icarus.2018.09.015.
16. Maxwell, R.E.; Garrick-Bethell, I. Evidence for an Ancient Near-Equatorial Lunar Dipole From Higher Precision Inversions of Crustal Magnetization. J Geophys Res-Planet 2020, 125, doi:10.1029/2020JE006567.
17. Oliveira, J.S.; Wieczorek, M.A. Testing the axial dipole hypothesis for the Moon by modeling the direction of crustal mag-netization. J Geophys Res-Planet 2017, 122, 383-399, doi:10.1002/2016je005199.
18. Ravat, D.; Purucker, M.E.; Olsen, N. Lunar Magnetic Field Models From Lunar Prospector and SELENE/Kaguya Along-Track Magnetic Field Gradients. J Geophys Res-Planet 2020, 125, doi:10.1029/2019JE006187.
19. Shibuya, H.; Tsunakawa, H.; Takahashi, F.; Shimizu, H.; Matsushima, M.; Team, K.M.L. Near surface magnetic field map-ping over the swirls in the SPA region using Kaguya LMAG data. In Proceedings of European Planetary Science Congress, 2010; pp. GP42A-03.
20. Tsunakawa, H.; Takahashi, F.; Shimizu, H.; Shibuya, H.; Matsushima, M. Surface vector mapping of magnetic anomalies over the Moon using Kaguya and Lunar Prospector observations. J Geophys Res-Planet 2015, 120, 1160-1185, doi:10.1002/2014je004785.
21. Wakita, S.; Johnson, B.C.; Garrick-Bethell, I.; Kelley, M.R.; Maxwell, R.E.; Davison, T.M. Impactor material records the an-cient lunar magnetic field in antipodal anomalies. Nature Communications 2021, 12, doi:10.1038/s41467-021-26860-1.
22. Crawford, D.A.; Schultz, P.H. Electromagnetic properties of impact-generated plasma, vapor and debris. International Journal of Impact Engineering 1999, 23, 169-180, doi:10.1016/s0734-743x(99)00070-6.
23. Hood, L.L. Central magnetic anomalies of Nectarian-aged lunar impact basins: Probable evidence for an early core dyna-mo. Icarus 2011, 211, 1109-1128, doi:10.1016/j.icarus.2010.08.012.
24. Hood, L.L.; Artemieva, N.A. Antipodal effects of lunar basin-forming impacts: Initial 3D simulations and comparisons with observations. Icarus 2008, 193, 485-502, doi:10.1016/j.icarus.2007.08.023.
25. Tikoo, S.M.; Gattacceca, J.; Swanson-Hysell, N.L.; Weiss, B.P.; Suavet, C.; Cournède, C. Preservation and detectability of shock-induced magnetization. J Geophys Res-Planet 2015, 120, 1461-1475, doi:10.1002/2015je004840.
26. Wieczorek, M.A.; Weiss, B.P.; Stewart, S.T. An Impactor Origin for Lunar Magnetic Anomalies. Science 2012, 335, 1212-1215, doi:10.1126/science.1214773.
27. Garrick-Bethell, I.; Weiss, B.P.; Shuster, D.L.; Tikoo, S.M.; Tremblay, M.M. Further evidence for early lunar magnetism from troctolite 76535. J Geophys Res-Planet 2017, 122, 76-93, doi:10.1002/2016je005154.

28. Hemingway, D.J.; Tikoo, S.M. Lunar Swirl Morphology Constrains the Geometry, Magnetization, and Origins of Lunar Magnetic Anomalies. J Geophys Res-Planet 2018, 123, 2223-2241, doi:10.1029/2018je005604.
29. Kelley, M.R.; Garrick-Bethell, I. Gravity constraints on the age and formation of the Moon's Reiner Gamma magnetic anomaly. Icarus 2020, 338, 113465, doi:10.1016/j.icarus.2019.113465.
30. Purucker, M.E.; Head, J.W.; Wilson, L. Magnetic signature of the lunar South Pole-Aitken basin: Character, origin, and age. J Geophys Res-Planet 2012, 117, doi:10.1029/2011je003922.
31. Bruck Syal, M.; Schultz, P.H. Cometary impact effects at the Moon: Implications for lunar swirl formation. Icarus 2015, 257, 194-206, doi:10.1016/j.icarus.2015.05.005.
32. Wieczorek, M.A.; Weiss, B.P.; Breuer, D.; Cébron, D.; Fuller, M.; Garrick-Bethell, I.; Gattacceca, J.; Halekas, J.S.; Hemingway, D.J.; Hood, L.L., et al. Lunar Magnetism. Reviews in Mineralogy and Geochemistry 2023, 89, 207-241, doi:10.2138/rmg.2023.89.05.
33. Yang, X.; Wieczorek, M. Magnetic signatures of lunar impact craters. Icarus 2024, 415, doi:10.1016/j.icarus.2024.116049.
34. Blewett, D.T.; Coman, E.I.; Hawke, B.R.; Gillis-Davis, J.J.; Purucker, M.E.; Hughes, C.G. Lunar swirls: Examining crustal magnetic anomalies and space weathering trends. Journal of Geophysical Research 2011, 116, doi:10.1029/2010je003656.
35. Hemingway, D.; Garrick-Bethell, I. Magnetic field direction and lunar swirl morphology: Insights from Airy and Reiner Gamma. J Geophys Res-Planet 2012, 117, doi:10.1029/2012je004165.
36. Lee, J.-K.; Maxwell, R.; Jin, H.; Baek, S.-M.; Ghassemi, O.; Kelley, M.; Lee, H.; Kim, K.-H.; Lee, S.; Garrick-Bethell, I. A small lunar swirl and its implications for the formation of the Reiner Gamma magnetic anomaly. Icarus 2019, 319, 869-884, doi:https://doi.org/10.1016/j.icarus.2018.09.015.
37. Schultz, P.H.; Srnka, L.J. Cometary collisions on the Moon and Mercury. Nature 1980, 284, 22-26.
38. Hood, L.L.; Schubert, G. Lunar Magnetic-Anomalies and Surface Optical-Properties. Science 1980, 208, 49-51, doi:DOI 10.1126/science.208.4439.49.
39. Hood, L.L.; Williams, C.R. The lunar swirls: distribution and possible origins. In Proceedings of Lunar and Planetary Sci-ence Conference, 1988; pp. 1988-1918.
40. Garrick-Bethell, I.; Lin, R.P.; Sanchez, H.; Jaroux, B.A.; Bester, M.; Brown, P.; Cosgrove, D.; Dougherty, M.K.; Halekas, J.S.; Hemingway, D. Lunar magnetic field measurements with a cubesat. In Proceedings of SPIE Defense, Security, and Sensing, 2013.
41. Hendrix, A.R.; Greathouse, T.K.; Retherford, K.D.; Mandt, K.E.; Gladstone, G.R.; Kaufmann, D.E.; Hurley, D.M.; Feldman, P.D.; Pryor, W.R.; Stern, S.A.; Cahill, J.T.S. Lunar swirls: Far-UV characteristics. Icarus 2016, 273, 68-74, doi:10.1016/j.icarus.2016.01.003.
42. Rüsch, O.; Hess, M.; Wöhler, C.; Bickel, V.T.; Marshal, R.M.; Patzek, M.; Huybrighs, H.L.F. Discovery of a Dust Sorting Pro-cess on Boulders Near the Reiner Gamma Swirl on the Moon. Journal of Geophysical Research: Planets 2024, 129, doi:10.1029/2023je007910.
43. Pieters, C.M.; Noble, S.K. Space weathering on airless bodies. J Geophys Res-Planet 2016, 121, 1865-1884, doi:10.1002/2016je005128.
44. Bamford, R.A.; Kellett, B.; Bradford, W.J.; Norberg, C.; Thornton, A.; Gibson, K.J.; Crawford, I.A.; Silva, L.; Gargaté, L.; Bingham, R. Minimagnetospheres above the Lunar Surface and the Formation of Lunar Swirls. Physical Review Letters 2012, 109, doi:10.1103/PhysRevLett.109.081101.
45. Deca, J.; Divin, A.; Lue, C.; Ahmadi, T.; Horányi, M. Reiner Gamma albedo features reproduced by modeling solar wind standoff. Communications Physics 2018, 1, 12.
46. Hood, L.; Coleman Jr, P.; Wilhelms, D. The Moon: Sources of the crustal magnetic anomalies. Science 1979, 204, 53-57.
47. Kurata, M.; Tsunakawa, H.; Saito, Y.; Shibuya, H.; Matsushima, M.; Shimizu, H. Mini-magnetosphere over the Reiner Gamma magnetic anomaly region on the Moon. Geophysical Research Letters 2005, 32, doi:10.1029/2005gl024097.
48. Blewett, D.T.; Halekas, J.; Ho, G.C.; Greenhagen, B.T.; Anderson, B.J.; Vines, S.K.; Regoli, L.; Jahn, J.M.; Kollmann, P.; Dene-vi, B.W. Lunar Vertex: PRISM Exploration of Reiner Gamma. In Proceedings of 53rd Lunar and Planetary Science Conference, 2022; p. 1131.
49. Denevi, B.W.; Robinson, M.S.; Boyd, A.K.; Sato, H.; Hapke, B.W.; Hawke, B.R. Characterization of space weathering from Lunar Reconnaissance Orbiter Camera ultraviolet observations of the Moon. Journal of Geophysical Research: Planets 2014, 119, 976-997, doi:10.1002/2013JE004527.

50. Kramer, G.Y.; Besse, S.; Nettles, J.; Combe, J.P.; Clark, R.N.; Pieters, C.M.; Staid, M.; Malaret, E.; Boardman, J.; Green, R.O. Newer views of the Moon: Comparing spectra from Clementine and the Moon Mineralogy Mapper. Journal of Geophysical Re-search: Planets 2011, 116, doi:10.1029/2010JE003728.
51. Oliveira, J.S.; Vervelidou, F.; Wieczorek, M.A.; Michelena, M.D. Constraints on the Spatial Distribution of Lunar Crustal Magnetic Sources From Orbital Magnetic Field Data. J Geophys Res-Planet 2024, 129, doi:10.1029/2023JE008125.
52. Hood, L.; Zakharian, A.; Halekas, J.; Mitchell, D.; Lin, R.; Acuña, M.; Binder, A. Initial mapping and interpretation of lunar crustal magnetic anomalies using Lunar Prospector magnetometer data. Journal of Geophysical Research: Planets 2001, 106, 27825-27839, doi:10.1029/2000JE001366.
53. Nicholas, J.B.; Purucker, M.E.; Sabaka, T.J. Age spot or youthful marking: Origin of Reiner Gamma. Geophysical Research Letters 2007, 34, L02205, doi:10.1029/2006gl027794.
54. Bando, Y.; Kumamoto, A.; Nakamura, N. Constraint on subsurface structures beneath Reiner Gamma on the Moon using the Kaguya Lunar Radar Sounder. Icarus 2015, 254, 144-149, doi:10.1016/j.icarus.2015.03.020.
55. Lemelin, M.; Lucey, P.G.; Miljkovic, K.; Gaddis, L.R.; Hare, T.; Ohtake, M. The compositions of the lunar crust and upper mantle: Spectral analysis of the inner rings of lunar impact basins. Planetary and Space Science 2019, 165, 230-243, doi:10.1016/j.pss.2018.10.003.
56. Lemelin, M.; Lucey, P.G.; Song, E.; Taylor, G.J. Lunar central peak mineralogy and iron content using the Kaguya Multi-band Imager: Reassessment of the compositional structure of the lunar crust. J Geophys Res-Planet 2015, 120, 869-887, doi:10.1002/2014je004778.
57. Taylor, L.A.; Pieters, C.; Patchen, A.; Taylor, D.H.S.; Morris, R.V.; Keller, L.P.; Mckay, D.S. Mineralogical and chemical characterization of lunar highland soils: Insights into the space weathering of soils on airless bodies. J Geophys Res-Planet 2010, 115, doi:10.1029/2009je003427.
58. Zhang, L.; Zhang, X.; Yang, M.; Xiao, X.; Qiu, D.; Yan, J.; Xiao, L.; Huang, J. New maps of major oxides and Mg # of the lu-nar surface from additional geochemical data of Chang'E-5 samples and KAGUYA multiband imager data. Icarus 2023, 397, doi:10.1016/j.icarus.2023.115505.
59. Cavanaugh, J.F.; Smith, J.C.; Sun, X.L.; Bartels, A.E.; Ramos-Izquierdo, L.; Krebs, D.J.; McGarry, J.F.; Trunzo, R.; No-vo-Gradac, A.M.; Britt, J.L., et al. The Mercury Laser Altimeter instrument for the MESSENGER mission. Space Science Reviews 2007, 131, 451-479, doi:10.1007/s11214-007-9273-4.
60. Smith, D.E.; Zuber, M.T.; Frey, H.V.; Garvin, J.B.; Head, J.W.; Muhleman, D.O.; Pettengill, G.H.; Phillips, R.J.; Solomon, S.C.; Zwally, H.J., et al. Mars Orbiter Laser Altimeter: Experiment summary after the first year of global mapping of Mars. J Geophys Res-Planet 2001, 106, 23689-23722, doi:Doi 10.1029/2000je001364.
61. Smith, D.E.; Zuber, M.T.; Neumann, G.A.; Lemoine, F.G.; Mazarico, E.; Torrence, M.H.; McGarry, J.F.; Rowlands, D.D.; Head, J.W.; Duxbury, T.H., et al. Initial observations from the Lunar Orbiter Laser Altimeter (LOLA). Geophysical Research Let-ters 2010, 37, doi:10.1029/2010gl043751.
62. Mazarico, E.; Rowlands, D.D.; Neumann, G.A.; Smith, D.E.; Torrence, M.H.; Lemoine, F.G.; Zuber, M.T. Orbit determination of the Lunar Reconnaissance Orbiter. Journal of Geodesy 2012, 86, 193-207, doi:10.1007/s00190-011-0509-4.
63. Barker, M.K.; Mazarico, E.; Neumann, G.A.; Zuber, M.T.; Haruyama, J.; Smith, D.E. A new lunar digital elevation model from the Lunar Orbiter Laser Altimeter and SELENE Terrain Camera. Icarus 2016, 273, 346-355, doi:10.1016/j.icarus.2015.07.039.
64. Liu, Q.; Cheng, W.; Yan, G. Distribution characteristics and classification schemes of lunar surface elevation. Acta Geo-graphica Sinica 2021, 76, 106-119, doi: 10.11821/dlxb202201008.
65. Deng, J. Classification of lunar landforms coupled with morphology and genesis and intelligent identification of impact landforms. University of Chinese Academy of Sciences, 2023.
66. Kreslavsky, M.A.; Head, J.W.; Neumann, G.A.; Rosenburg, M.A.; Aharonson, O.; Smith, D.E.; Zuber, M.T. Lunar topograph-ic roughness maps from Lunar Orbiter Laser Altimeter (LOLA) data: Scale dependence and correlation with geologic features and units. Icarus 2013, 226, 52-66, doi:10.1016/j.icarus.2013.04.027.
67. Deng, J.Y.; Cheng, W.M.; Liu, Q.Y.; Jiao, Y.M.; Liu, J.Z. Morphological differentiation characteristics and classification crite-ria of lunar surface relief amplitude. Journal of Geographical Sciences 2022, 32, 2365-2378, doi:10.1007/s11442-022-2052-z.
68. Bandfield, J.L.; Hayne, P.; Williams, J.P.; Greenhagen, B.T.; Paige, D.A. Lunar surface roughness derived from LRO Diviner Radiometer observations. Icarus 2015, 248, 357-372, doi:10.1016/j.icarus.2014.11.009.

69. Chen, J.; Ling, Z.C.; Liu, J.Z.; Chen, S.B.; Ding, X.Z.; Chen, J.P.; Cheng, W.M.; Li, B.; Zhang, J.; Sun, L.Z., et al. Digital and global lithologic mapping of the Moon at a 1:2,500,000 scale. Science Bulletin 2022, 67, 2050-2054, doi:10.1016/j.scib.2022.09.015.
70. Guo, D.; Liu, J.; Head, J.W.; Zhang, F.; Ling, Z.; Chen, S.; Chen, J.; Ding, X.; Ji, J.; Ouyang, Z. A lunar time scale from the perspective of the Moon's dynamic evolution. Science China Earth Sciences 2023, 67, 234-251, doi:10.1007/s11430-022-1183-4.
71. Ji, J.Z.; Guo, D.J.; Liu, J.Z.; Chen, S.B.; Ling, Z.C.; Ding, X.Z.; Han, K.Y.; Chen, J.P.; Cheng, W.M.; Zhu, K., et al. The 1:2,500,000-scale geologic map of the global Moon. Science Bulletin 2022, 67, 1544-1548, doi:10.1016/j.scib.2022.05.021.
72. Liu, J.; Liu, J.; Yue, Z.; Zhang, L.; Wang, J.; Zhu, K. Characterization and interpretation of the global lunar impact basins based on remote sensing. Icarus 2022, 378, 114952, doi:10.1016/j.icarus.2022.114952.
73. Lu, T.Q.; Zhu, K.; Chen, S.B.; Liu, J.Z.; Ling, Z.C.; Ding, X.Z.; Han, K.Y.; Chen, J.P.; Cheng, W.M.; Lei, D.H., et al. The 1:2,500,000-scale global tectonic map of the Moon. Science Bulletin 2022, 67, 1962-1966, doi:10.1016/j.scib.2022.08.017.
74. Hiesinger, H.; Head, J.W.; Wolf, U.; Jaumann, R.; Neukum, G. Ages and stratigraphy of mare basalts in Oceanus Procella-rum, Mare Nubium, Mare Cognitum, and Mare Insularum. J Geophys Res-Planet 2003, 108, doi:10.1029/2002je001985.
75. Hiesinger, H.; Head, J.W.; Wolf, U.; Jaumann, R.; Neukum, G. Ages and stratigraphy of lunar mare basalts: a synthesis. In Recent Advances and Current Research Issues in Lunar Stratigraphy, Geol. Soc. Am. Bull.: 2011; pp. 1-52.
76. Taylor, L.A.; Pieters, C.M.; Keller, L.P.; Morris, R.V.; McKay, D.S. Lunar Mare Soils: Space weathering and the major effects of surface-correlated nanophase Fe. J Geophys Res-Planet 2001, 106, 27985-27999, doi:Doi 10.1029/2000je001402.
77. Deca, J.; Hemingway, D.J.; Divin, A.; Lue, C.; Poppe, A.R.; Garrick-Bethell, I.; Lembège, B.; Horányi, M. Simulating the Reiner Gamma Swirl: The Long-Term Effect of Solar Wind Standoff. J Geophys Res-Planet 2020, 125, doi:10.1029/2019JE006219.
78. Deca, J.; Poppe, A.R.; Divin, A.; Lembège, B. The Plasma Environment Surrounding the Reiner Gamma Magnetic Anomaly. Journal of Geophysical Research-Space Physics 2021, 126, doi:10.1029/2021JA029180.
79. Jiang, Z.; ZongCheng, L.; Bo, L.; ZhongChen, W. Photometric behaviors and classification of Reiner Gamma swirl materi-als. Acta Petrologica Sinica 2016, 32, 113-118.
80. Poppe, A.R.; Fatemi, S.; Garrick-Bethell, I.; Hemingway, D.; Holmström, M. Solar wind interaction with the Reiner Gamma crustal magnetic anomaly: Connecting source magnetization to surface weathering. Icarus 2016, 266, 261-266, doi:10.1016/j.icarus.2015.11.005.
81. Walker, R.T.; Barker, M.K.; Mazarico, E.; Sun, X.; Neumann, G.A.; Smith, D.E.; Head, J.W.; Zuber, M.T. Near-infrared Pho-tometry of the Moon's Surface with Passive Radiometry from the Lunar Orbiter Laser Altimeter (LOLA). The Planetary Science Journal 2024, 5, 122, doi:10.3847/PSJ/ad4467.
82. Carporzen, L.; Weiss, B.P.; Elkins-Tanton, L.T.; Shuster, D.L.; Ebel, D.; Gattacceca, J. Magnetic evidence for a partially dif-ferentiated carbonaceous chondrite parent body. Proceedings of the National Academy of Sciences of the United States of Amer-ica 2011, 108, 6386-6389, doi:10.1073/pnas.1017165108.
83. Cournede, C.; Gattacceca, J.; Gounelle, M.; Rochette, P.; Weiss, B.P.; Zanda, B. An early solar system magnetic field record-ed in CM chondrites. Earth and Planetary Science Letters 2015, 410, 62-74, doi:10.1016/j.epsl.2014.11.019.
84. Fu, R.R.; Lima, E.A.; Weiss, B.P. No nebular magnetization in the Allende CV carbonaceous chondrite. Earth and Planetary Science Letters 2014, 404, 54-66, doi:10.1016/j.epsl.2014.07.014.
85. Weiss, B.P.; Berdahl, J.S.; Elkins-Tanton, L.; Stanley, S.; Lima, E.A.; Carporzen, L. Magnetism on the Angrite Parent Body and the Early Differentiation of Planetesimals. Science 2008, 322, 713-716, doi:10.1126/science.1162459.
86. Zhang, Y.C.; Stevens, J.G.; Li, Y.S.; Li, Z.L. Mossbauer Study of the Jilin and Xinyang Meteorites. Hyperfine Interactions 1994, 91, 547-550, doi:Doi 10.1007/Bf02064568.
87. Borg, L.E.; Cassata, W.S.; Wimpenny, J.; Gaffney, A.M.; Shearer, C.K. The formation and evolution of the Moon's crust in-ferred from the Sm-Nd isotopic systematics of highlands rocks. Geochim Cosmochim Ac 2020, 290, 312-332, doi:10.1016/j.gca.2020.09.013.

88. Charlier, B.; Grove, T.L.; Namur, O.; Holtz, F. Crystallization of the lunar magma ocean and the primordial mantle-crust differentiation of the Moon. Geochim Cosmochim Ac 2018, 234, 50-69, doi:10.1016/j.gca.2018.05.006.
89. Johnson, T.E.; Morrissey, L.J.; Nemchin, A.A.; Gardiner, N.J.; Snape, J.F. The phases of the Moon: Modelling crystallisation of the lunar magma ocean through equilibrium thermodynamics. Earth and Planetary Science Letters 2021, 556, 116721, doi:10.1016/j.epsl.2020.116721.
90. Rapp, J.F.; Draper, D.S. Fractional crystallization of the lunar magma ocean: Updating the dominant paradigm. Meteorit Planet Sci 2018, 53, 1432-1455, doi:10.1111/maps.13086.
91. Snyder, G.A.; Taylor, L.A.; Neal, C.R. A Chemical-Model for Generating the Sources of Mare Basalts - Combined Equilib-rium and Fractional Crystallization of the Lunar Magmasphere. Geochim Cosmochim Ac 1992, 56, 3809-3823, doi:Doi 10.1016/0016-7037(92)90172-F.
92. Wieczorek, M.A.; Neumann, G.A.; Nimmo, F.; Kiefer, W.S.; Taylor, G.J.; Melosh, H.J.; Phillips, R.J.; Solomon, S.C.; An-drews-Hanna, J.C.; Asmar, S.W., et al. The Crust of the Moon as Seen by GRAIL. Science 2013, 339, 671-675, doi:10.1126/science.1231530.
93. Borg, L.E.; Shearer, C.K.; Asmerom, Y.; Papike, J.J. Prolonged KREEP magmatism on the Moon indicated by the youngest dated lunar igneous rock. Nature 2004, 432, 209-211, doi:10.1038/nature03070.
94. Elardo, S.M.; Laneuville, M.; McCubbin, F.M.; Shearer, C.K. Early crust building enhanced on the Moon's nearside by man-tle melting-point depression. Nature Geoscience 2020, 13, 339-343, doi:10.1038/s41561-020-0559-4.
95. Lin, Y.H.; Tronche, E.J.; Steenstra, E.S.; van Westrenen, W. Experimental constraints on the solidification of a nominally dry lunar magma ocean. Earth and Planetary Science Letters 2017, 471, 104-116, doi:10.1016/j.epsl.2017.04.045.
96. Shearer, C.K.; Elardo, S.M.; Petro, N.E.; Borg, L.E.; McCubbin, F.M. Origin of the lunar highlands Mg-suite: An integrated petrology, geochemistry, chronology, and remote sensing perspective. American Mineralogist 2015, 100, 294-325, doi:10.2138/am-2015-4817.
97. Whitten, J.; Head, J.W.; Staid, M.; Pieters, C.M.; Mustard, J.; Clark, R.; Nettles, J.; Klima, R.L.; Taylor, L. Lunar mare deposits associated with the Orientale impact basin: New insights into mineralogy, history, mode of emplacement, and relation to Ori-entale Basin evolution from Moon Mineralogy Mapper (M3) data from Chandrayaan-1. Journal of Geophysical Research 2011, 116, doi:10.1029/2010je003736.
98. Whitten, J.L.; Head, J.W. Lunar cryptomaria: Physical characteristics, distribution, and implications for ancient volcanism. Icarus 2015, 247, 150-171, doi:10.1016/j.icarus.2014.09.031.
99. Shea, E.K.; Weiss, B.P.; Cassata, W.S.; Shuster, D.L.; Tikoo, S.M.; Gattacceca, J.; Grove, T.L.; Fuller, M.D. A Long-Lived Lunar Core Dynamo. Science 2012, 335, 453-456, doi:10.1126/science.1215359.
100. Suavet, C.; Weiss, B.P.; Cassata, W.S.; Shuster, D.L.; Gattacceca, J.; Chan, L.; Garrick-Bethell, I.; Head, J.W.; Grove, T.L.; Fuller, M.D. Persistence and origin of the lunar core dynamo. Proceedings of the National Academy of Sciences of the United States of America 2013, 110, 8453-8458, doi:10.1073/pnas.1300341110.
101. Tikoo, S.M.; Weiss, B.P.; Buz, J.; Lima, E.A.; Shea, E.K.; Melo, G.; Grove, T.L. Magnetic fidelity of lunar samples and impli-cations for an ancient core dynamo. Earth and Planetary Science Letters 2012, 337, 93-103, doi:10.1016/j.epsl.2012.05.024.
102. Hiesinger, M.H.; Gebhart, J.; van der Bogert, C.; Pasckert, J.; Weinauer, J.; Lawrence, S.; Stopar, J.; Robinson, M. Stratigra-phy of low shields and mare basalts of the Marius Hills region. In Proceedings of Lunar Planet. Sci. Conf., 2016.
103. Lawrence, S.J.; Stopar, J.D.; Hawke, B.R.; Greenhagen, B.T.; Cahill, J.T.; Bandfield, J.L.; Jolliff, B.L.; Denevi, B.W.; Robinson, M.S.; Glotch, T.D. LRO observations of morphology and surface roughness of volcanic cones and lobate lava flows in the Marius Hills. Journal of Geophysical Research: Planets 2013, 118, 615-634.
104. Tikoo, S.M.; Weiss, B.P.; Cassata, W.S.; Shuster, D.L.; Gattacceca, J.; Lima, E.A.; Suavet, C.; Nimmo, F.; Fuller, M.D. Decline of the lunar core dynamo. Earth and Planetary Science Letters 2014, 404, 89-97, doi:10.1016/j.epsl.2014.07.010